Journal of Hydrology 476 (2013) 42–51

Contents lists available at SciVerse ScienceDirect

Journal of Hydrology

journal homepage: www.elsevier.com/locate/jhydrol

Estimating actual evapotranspiration from an alpine grassland on Qinghai-Tibetan plateau using a two-source model and parameter uncertainty analysis by Bayesian approach

Zhu Gaofeng [a,*], Su Yonghong [b,2,3], Li Xin [c,2,4], Zhang Kun [a,1,5], Li Changbin [a,1,6]

[a] Center for Dryland Water Resources Research and Watershed Science, Key Laboratory of Western China's Environmental Systems (Ministry of Education), Lanzhou University, PR China
[b] Division of Hydrology Water-Land Research in Cold and Arid Regions, Cold and Arid Regions Environmental and Engineering Research Institute, CAS, PR China
[c] Laboratory of Remote Sensing and Geospatial Science, Cold and Arid Regions Environmental and Engineering Research Institute, CAS, PR China

ARTICLE INFO

Article history:
Received 29 May 2012
Received in revised form 18 September 2012
Accepted 11 October 2012
Available online 30 October 2012
This manuscript was handled by Peter K. Kitanidis, Editor-in-Chief, with the assistance of Markus Tuller, Associate Editor

Keywords:
Bayesian statistics
Evapotranspiration
Shuttleworth–Wallace model
Alpine grassland
Qinghai-Tibetan plateau

SUMMARY

A Bayesian method was used to fit the Shuttleworth–Wallace model to half-hourly measurements of evapotranspiration (ET) with the eddy covariance technique from an alpine grassland on the Qinghai-Tibetan plateau during the main growing season in 2008, and probabilistically estimated its parameters and predication uncertainties using both dataset-by-dataset and multi-data procedures. This enabled us to reveal the seasonal variations of some physiology-related parameters and the impacts of constant parameters on the performances of the model. Results indicated that the S–W model using the posterior mean parameter values obtained by different procedures all successfully reproduced the observed responses in ET. However, the seasonal variations in the canopy conductance parameter (g_{max}) should be counted in long-term ET estimating. From simulated results, the daily mean partitioning [i.e. the ratio of the estimated daily soil evaporation (E) over total evapotranspiration (ET); E/ET] was relative low (0.02–0.07 with a mean of 0.04) for the alpine grassland when leaf area index (LAI) was more than 3 m^2 m^{-2}, and was closed related to LAI and vegetation condition. At the diurnal timescale, the canopy conductance was the main factor control the partitioning of ET.

1. Introductions

Evapotranspiration (ET), which is composed of vegetation transpiration (T) and soil water evaporation (E), is an important land surface process in climatology and a nexus for terrestrial carbon and energy cycles (Jung et al., 2010). Therefore, ET estimates are crucial to a wide range of problems in hydrology (Xu and Singh, 1998), geographical ecology (Fisher et al., 2011), global change studies (Reynolds et al., 2000) and practical applications. Generally, ET and its components can be directly measured by lysimeter, sap flow, eddy covariance (EC) and stable isotope techniques (Williams et al., 2004; Moran et al., 2009) but expensively and labor-intensively (Gasca-Tucker et al., 2007). On the other hand, numerous models, from the single climatic variable driven equations to energy balance and aerodynamic principle combination methods [see Xu and Singh (1998) for a comprehensive review], have been developed for estimating ET, and are becoming more and more popular (Shugart, 2000). Among them, the Shuttleworth–Wallace (S–W) model, in which the interactions between the fluxes from soil and canopy are taken into account, is physically sound and rigorous, and is more suitable for estimating ET from complex or seasonally changing vegetation covers (Kato et al., 2004; Hu et al., 2009).

Although the S–W model has been widely used in estimating ET from various plant types over small experiment catchments (e.g., Iritz et al., 1999 among others) or in the water balance model at a continent (Vorosmarty et al., 1998), there are still some insufficiencies in the application of the S–W model (Hu et al., 2009). First, the S–W model is highly complex with many site- or species-specific parameters that needed to be calibrated with observed data (Zhou et al., 2006). Traditionally, the parameters in the S–W model were obtained by fitting the model to (a series of) ecosystem-level ET observations through 'trial and error' procedures: the model is re-run with different sets of parameter values until observations are reproduced well (e.g., Leuning et al., 2008; Hu

* Corresponding author. Address: 222 South Tianshui Road, Lanzhou, Gansu Province 730000, PR China. Tel.: +86 931 8912812; fax: +86 931 8912856.
E-mail addresses: zhugf@lzu.edu.cn (G. Zhu), syh@lzb.ac.cn (Y. Su), lixin@lzb.ac.cn (X. Li), zhkgis@163.com (K. Zhang), licb@lzu.edu.cn (C. Li).
[1] Address: 222 South Tianshui Road, Lanzhou, Gansu Province 730000, PR China.
[2] Address: 320 West Donggang Road, Lanzhou, Gansu Province 730000, PR China.
[3] Tel.: +86 931 4967094; fax: +86 931 4967152.
[4] Tel.: +86 931 4967249; fax: +86 931 8279161.
[5] Tel.: +86 931 8912812; fax: +86 931 8912856.
[6] Tel./fax: +86 931 8912856.

0022-1694/$ - see front matter © 2012 Elsevier B.V. All rights reserved.
http://dx.doi.org/10.1016/j.jhydrol.2012.10.006

et al., 2009). However, in a deterministic model with multiple parameters, several combinations of input parameters may give similar model result, which hampers the identification of a unique set of parameters (Reinds et al., 2008). Thus, it is more reasonable to treat the parameters as probability distributions rather than fixed values (Larssen et al., 2006). In addition, the traditional calibration methods do not take into account the uncertainty in the parameters, model structure and observations (Reinds et al., 2008). Relatively recently, the Bayesian approach has been introduced to combine probability distributions of model parameters, based on prior assumptions about their magnitude and uncertainty, with measurements to generate posterior distributions of parameters. This not only allows quantifying uncertainty in inputs, parameters and outputs of models, but also allows considering prior knowledge for all parameters and accommodating unknown influences (Clark and Gelfand, 2006; Zhu et al., 2011). Abundant evidence has shown that the Bayesian approach provides powerful new tools to draw inference on high-dimensional models (Clark and Gelfand, 2006). However, the use of Bayesian approach with the S–W model is relatively rare, probably due to the higher dimensionality of the parameter spaces as compared to other evapotranspiration models (e.g., the Penman–Monteith model; Samanta et al., 2007). The second problem is that some parameters in the S–W model were closely related to the physiological state of the plant and therefore they can exhibit some seasonal fluctuations during the whole growing stage (Wever et al., 2002). However, the pattern of seasonal variations of the physiology-related parameters is critically limited for the alpine grasslands. Furthermore, although the partitioning of ET using the S–W model and its controls were investigated by several authors (e.g., Kato et al., 2004; Sauer et al., 2007; Hu et al., 2009), studies based on long-term performance of the model over a wide type of ecosystem under various climatic conditions are still needed (Hu et al., 2009).

In this study, we applied the Bayesian approach to calibrate the S–W model on the alpine grassland on the Qinghai-Tibetan Plateau, which is one of the most sensitive regions to climate change (Liu and Chen, 2000). The S–W model were calibrated using: (i) seasonal EC-measured ET data in different growing stages, called 'dataset-by-dataset calibration' hereafter, and (ii) the entire ET data during the whole growing season, called 'multi-data calibration'. In this way, we can investigate the seasonal fluctuations of parameters in the S–W model, and the impact of fixed parameters throughout the investigated period on the performances of the model. Also, the partitioning of ET and its controls in the alpine grassland were investigated and compared with other ecosystems. It is expected that this study can improve our understandings not only about hydrological cycle in the alpine ecosystem, but also the impacts of climate change on the water balance in the highest plateau of the world.

2. Methods and materials

2.1. Study site

The study site is located at Arou freeze/thaw observation station (lat. 38°02′N, long. 100°27′E) in the Qilian Mountains of the Qinghai-Tibetan plateau, China. The elevation is 2995 m above sea level. The annual average temperature and precipitation for 1990–2000 were −0.2 °C and 411.3 mm (Niu et al., 2008), respectively. The soil is classified as subalpine meadow soil with an average thickness of about 1 m (Chang et al., 2009), are wet high in organic matter (ca. 14.6%).

The plant community with a height of 20–30 cm is dominated mainly by four perennial herbs, *Carex*, *Stipa grandi*, *Leontopodium* and *Potentillal*, and by alpine patchy shrub species, *Potentilla fruticasa*, *Caragana jubata* and *Salix gilashaniea*. The grassland turns green at the end of May and becomes senescence in early or middle October, depending on the climate of a given year.

2.2. Measurements

The site was set up and instrumented in June 2008 as part of the Watershed Allied Telemetry Experimental Research (WATER) project (see details in Li et al., 2009 and Supporting information A). Net ecosystem water vapor and carbon dioxide gas exchange was measured at the height 2 m using the eddy covariance system, which consists of a 3D sonic anemometer (CSAT-3, Campbell Scientific Inc. Logan, UT, USA) and an open-path CO_2/H_2O gas analyzer (Li-7500, LiCor Inc., USA). The signals were recorded at a rate of 10 Hz by a datalogger (Campbell Scientific Inc. Logan, UT, USA) and then block-averaged over 30-min intervals. Post-processing calculations, using the TK2 software package (Mauder and Foken, 2004), included the WPL density fluctuation correction, spectral loss correction, planar fit coordinate rotation, sonic virtual temperature conversion, and spike detection. Following the procedure in the LI-COR Instruction Manual (Li-COR Inc., 2000), the CO_2/H_2O analyzer system was calibrated every year at the beginning of the growing season. Zero points were established using dry N_2 gas, the CO_2 span was calibrated using a standard gas bottle of CO_2 (303.3 607.7 and 1000 ppmv standard CO_2 gases) and the water vapor using a dew-poing generator (Li-610; Li-COR Inc., NE, USA).

Continuous complementary measurements also included standard climatological and soil temperatures. Rainfall was measuring using a tipping bucket rain gauge (TE525MM, Campbell Scientific Instruments Inc.). Air temperature and relative humidity (HMP45C, Vaisala Inc., Helsinki, Finland) were measured at heights of 2 and 10 m above the ground. Wind speed and direction (034B, Met One Instruments, Inc. USA) were measured at the height of 10 m. Downward and upward solar and longwave radiation (PSP, The EPPLEY Laboratory Inc., USA) and photosynthetic photon flux density (PPFD) (LI-190SA, LI-COR Inc.) were measured at height of 1.5 m. Soil temperature (Campbell-107, Campbell Scientific Instruments Inc.) and moisture (CS616, Campbell Scientific Instruments Inc.) were measured at 0.1, 0.2, 0.4, 0.8, 1.2 and 1.6 m depths. Soil heat fluxes were measured at the depths of 0.05 and 0.15 m (HFT3, Campbell Scientific Instruments Inc.). These data were logged every 30 min by a digital micrologger (CR23X, Campbell Scientific Inc.) equipped with an analog multiplexer (AM416) was used for sampling and logging data. Leaf area index (LAI) was measured by harvesting the vegetation approximately every 2 weeks during the growing season, and the gaps were linearly interpolated to daily interval.

2.3. Shuttleworth–Wallace (S–W) model

In the S–W model, the ecosystem evapotranspiration (λET is separated into evaporation from the soil surface (λE) and transpiration from the canopy (λT) (Fig. 1). The total evapotranspiration and each term are expressed (Shuttleworth and Wallace, 1985) as:

$$\lambda \mathrm{ET} = \lambda E + \lambda T = C_s \mathrm{ET}_s + C_c \mathrm{ET}_c \tag{1}$$

$$\mathrm{ET}_s = \frac{\Delta A + \{\rho C_p (e_s - e_a) - \Delta r_{as}(A - A_s)\}/(r_{aa} + r_{as})}{\Delta + \gamma\{1 + r_{ss}/(r_{aa} + r_{as})\}} \tag{2}$$

$$\mathrm{ET}_c = \frac{\Delta A + \{\rho C_p (e_s - e_a) - \Delta r_{ac} A_s\}/(r_{aa} + r_{ac})}{\Delta + \gamma\{1 + r_{sc}/(r_{aa} + r_{ac})\}} \tag{3}$$

where ET_s and ET_c, are terms similar to that in the Penman–Monteith (Monteith, 1965) model to describe soil evaporation and

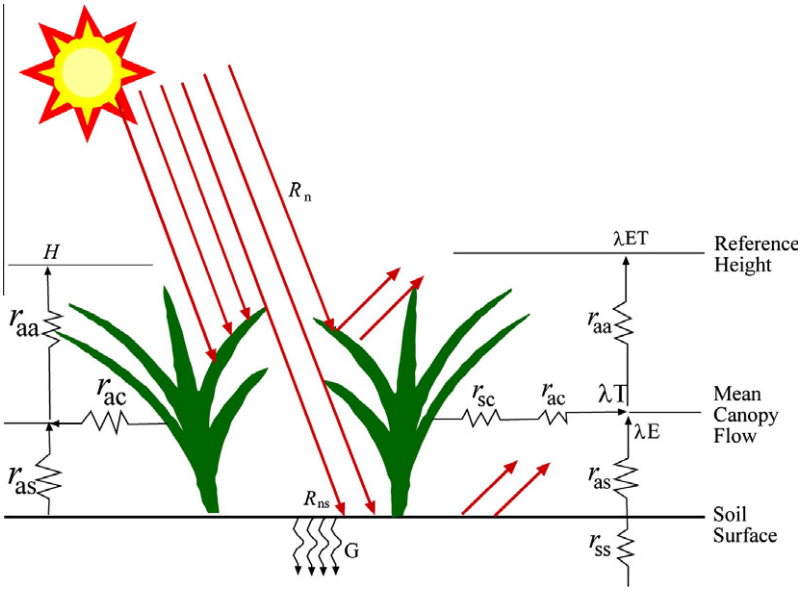

Fig. 1. Schematic diagram of the S–W model. From right to left, r_{sc} and r_{ac} bulk resistances of canopy stomatal and boundary layer, respectively; r_{as} and r_{aa} aerodynamic resistances from soil to canopy and from canopy to reference height, respectively; r_{ss} soil surface resistance; R_n and R_{ns} net radiations above canopy and to soil surface, respectively; G soil heat flux, λT transpiration from canopy, λE evaporation from soil, λET total evapotranspiration, and H sensible heat.

canopy transpiration (W m^{-2}), respectively; C_s and C_c are the soil surface resistance coefficient and canopy resistance coefficient (dimensionless), respectively; λ is the latent heat of water vaporisation (MJ kg^{-1}); Δ is the slope of the saturation vapor pressure versus temperature curve (kPa K^{-1}); ρ is air density (kg m^{-3}); C_p is the specific heat at constant pressure (1013 J kg^{-1} K^{-1}); e_s and e_a are the saturated and actual vapor pressures (kPa) at the reference height (2 m), respectively; γ is the psychrometric constant (kPa K^{-1}); r_{sc} and r_{ac} are bulk resistances (s m^{-1}) of canopy stomatal and boundary layer, respectively; r_{as} and r_{aa} are aerodynamic resistances (s m^{-1}) from soil to canopy and from canopy to reference height, respectively; r_{ss} are soil surface resistance(s m^{-1}). Calculations of the five resistances will be addressed later. A and A_s are the available energy (W m^{-2}) input above the canopy and above the soil surface, respectively, and are defined as follows:

$$A = R_n - G \tag{4}$$

$$A_s = R_{ns} - G \tag{5}$$

where R_n and R_{ns} are net radiation fluxes into the canopy and the substrate (W m^{-2}), respectively; G is the soil heat flux (W m^{-2}). The radiation reaching soil surface, R_{ns}, can be calculated using a Beer's law relationship of the form:

$$R_{ns} = R_n \exp(-K_A \mathrm{LAI}) \tag{6}$$

in which K_A is the extinction coefficient of light attenuation, and LAI is the total leaf area index.

In Eq. (1), the two coefficients C_s and C_c are obtained as follows:

$$C_s = \frac{1}{1 + R_s R_a/(R_c(R_s + R_a))} \tag{7}$$

$$C_c = \frac{1}{1 + R_c R_a/(R_s(R_c + R_a))} \tag{8}$$

in which R_a, R_s and R_c are calculated as:

$$R_a = (\Delta + \gamma) r_{aa} \tag{9}$$

$$R_s = (\Delta + \gamma) r_{as} + \gamma r_{ss} \tag{10}$$

$$R_c = (\Delta + \gamma) r_{ac} + \gamma r_{sc} \tag{11}$$

In Eqs. (1)–(3), parameters λ, e_s, Δ, ρ and γ are directly related to the climatic variables, which is calculated by the formula of Allen et al. (1998):

$$\lambda = 2.501 - 0.002361 T_a \tag{12}$$

$$e_s(T_a) = 0.6108 \exp\left(\frac{17.27 T_a}{T_a + 237.3}\right) \tag{13}$$

$$\Delta = \frac{4098\left[0.6108 \exp\left(\frac{17.27 T_a}{T_a + 237.3}\right)\right]}{(T_a + 237.3)^2} \tag{14}$$

$$\rho = \frac{P}{R T_{kv}} \tag{15}$$

$$\gamma = \frac{C_p P}{\varepsilon \lambda} \tag{16}$$

where T_a is the air temperature (°C) at the reference height; P is the atmospheric pressure (kPa); T_{KV} is the air virtual temperature (K), $T_{KV} = 1.01(273 + T_a)$; R is the specific gas constant (287 J kg^{-1} K^{-1}); ε is the ratio between the molecular weights of water vapor and air (0.622).

2.4. Calculation of resistances in the S–W model

Different methods have been proposed to calculate the five resistances involved in the S–W model (Fig. 1). The performances of different parameterization methods for each resistance were compared (given in Supporting information B). In our paper, the two aerodynamic resistance (i.e., r_{aa} and r_{as}; Fig. 1) was modeled following the approach proposed by Shuttleworth and Wallace (1985), and the boundary layer resistance (r_{ac}; Fig. 1) was parameterized as suggested by Shuttleworth and Gurney (1990) (also see Supporting information B).

Soil surface resistance (r_{ss}; Fig. 1) was expressed as a function of near-surface soil water content (Sellers et al., 1992):

$$r_{ss} = \exp\left(b_1 - b_2\frac{\theta}{\theta_s}\right) \quad (17)$$

in which b_1 (s m^{-1}) and b_2 (s m^{-1}) are empirical constants; θ the soil water content (m^3 m^{-3}) at a depth of 5 cm, and θ_s is the saturated water content (m^3 m^{-3}), which was estimated empirically through the near-surface soil texture.

In many problems it is more convenient to work with the reciprocal of the bulk stomatal resistance (r_{sc}), known as canopy conductance (g_{sc}). The expression for canopy conductance (g_{sc}) developed by Leuning et al. (2008) was given as:

$$g_{sc} = \frac{g_{max}}{K_Q}\ln\left[\frac{Q_h + Q_{50}}{Q_h\exp(-K_Q LAI) + Q_{50}}\right]\left[\frac{1}{1 + D_a/D_{50}}\right] \quad (18)$$

in which g_{max} is the maximum stomatal conductance of leaves at the top of the canopy (m s^{-1}); K_Q is the extinction coefficient for shortwave radiation; Q_h is the flux density of visible radiation at the top of the canopy (W m^{-2}) (approximately half of incoming solar radiation); Q_{50} is the visible radiation flux when stomatal conductance is half its maximum value (W m^{-2}); D_a is the vapor pressure deficit (VPD) at the reference height (kPa); and D_{50} is the VPD at which stomatal conductance is half its maximum value (kPa). The responses of g_{sc} to VPD, LAI and solar radiation calculated by the formula suggested by Leuning et al. (2008) were similar to that by means of the multiplicative formulation proposed by Jarvis (1976) (see Supporting information B). To include the effect of soil water content on stomatal conductance, we modified this expression (Eq. (18)) as:

$$g_{sc} = \frac{g_{max}}{K_Q}\ln\left[\frac{Q_h + Q_{50}}{Q_h\exp(-K_Q LAI) + Q_{50}}\right]\left[\frac{1}{1 + D_a/D_{50}}\right]f(\theta) \quad (19)$$

where $f(\theta)$ is the factor that takes into account water stress, and it ranges between 0 and 1 following the relationship (Thompson et al., 1981):

$$f(\theta) = \begin{cases} 1 & \theta > \theta_{cr} \\ \frac{\theta-\theta_w}{\theta_{cr}-\theta_w} & \theta_w \leqslant \theta \leqslant \theta_{cr} \\ 0 & \theta < \theta_w \end{cases} \quad (20)$$

where θ_w is water content at the wilting point (m^3 m^{-3}); and θ_{cr} is the critical water content at which plant stress starts and was set as $\theta_{cr} = 0.75\theta_s$.

2.5. Model calibration and evaluation of model predications

The parameters associated with the S–W model described above, namely K_A, b_1, b_2, g_{max}, K_Q, Q_{50} and D_{50} (Table 1), were components of the parameter vector, β, and were calibrated using the Bayesian probabilistic inversion approach. We assumed that the model error, i.e. the difference between the simulated outputs (S) and observed data (O), is independent and normally distributed with mean zero (Van Oijen et al., 2005; Svensson et al., 2008; Zhu et al., 2011). From the properties of the normal distribution, the likelihood function for the entire series O, containing n observations, is calculated as:

$$p(O|\beta,\sigma^2) \propto \sigma^{-n}\prod_{i=1}^{n}\exp\left\{-\frac{[O_i - S(x_i,\beta)]^2}{2\sigma^2}\right\} \quad (21)$$

where O_i is the measured evapotranspiration flux for observation i ($i = 1,2,\ldots,n$), x_i is the vector of model input data, $S(x_i;\beta)$ is the model simulation output with the parameter vector β, and σ is the standard deviation of the model error. We assumed that the calibration parameter (β) is distributed uniformly within a specified interval (Table 1), and the prior distribution of σ is uniform over $\log\sigma$ (Gelman et al., 1995). Thus, the noninformative prior distribution used in our analysis was:

$$p(\beta,\sigma^2) \propto \frac{1}{\sigma^2} \quad (22)$$

Using the above prior, the joint posterior distribution, also called the target distribution, is defined as:

$$p(\beta,\sigma^2|O) \propto \sigma^{-(n+2)}\prod_{i=1}^{n}\exp\left\{-\frac{[O_i - S(x_i;\beta)]^2}{2\sigma^2}\right\} \quad (23)$$

The posterior distribution was sampled using the Metropolis–Hasting (M–H) algorithm (Metropolis et al., 1953; Hastings, 1970), a version of the Markov Chain Monte Carlo (MCMC) technique (Gelfand and Smith, 1990; Gelman and Rubin, 1992). To generate a Markov chain in the parameter space, the M–H algorithm was run by repeating two steps: a proposing step and a moving step. In the proposing step, we used a uniform proposal distribution to generate a new point β^{new} centered at the previously accepted point $\beta^{(k-1)}$:

$$\beta^{new} = \beta^{(k-1)} + \frac{u}{D}\times(\beta^{max} - \beta^{min}) \quad (24)$$

where u is a random number uniformly distributed between −0.5 and +0.5, β^{max} and β^{min} is the upper and lower limits of parameter vector β, and D is a value controlling the proposing step size. In the moving step, point β^{max} is treated against the Metropolis criterion to examine if it should be accepted or rejected (see Supporting information C for a detail description of the M–H algorithm). The Bayesian calibration procedure was written in the computer programming language Matlab 7.3 (MatWorks Inc., Natick, MA, USA). We ran at least three parallel MCMC chains with 20000 iterations each, evaluated the chains for convergence, and thinned the chains (every 20th iteration) when appropriate to reduce within chain autocorrelation, thereby producing an independent sample of 3000 values for each parameter from the joint posterior distribution.

2.6. Evaluation of model predictions

Model goodness-of-fit was evaluated by using the S–W model to predict evapotranspiration, which could then be compared with measured values. If the model perfectly predicted the data, all observed-versus-predicted points would lie exactly on the 1:1 line. We also used the root mean square error (RMSE) to characterize the mismatch of the calculated values against the observed values. The RMSE is given by:

$$\mathrm{RMSE} = \sqrt{\frac{1}{n}\sum_{i=1}^{n}[O_i - S(x_i;\bar{\beta})]^2} \quad (25)$$

where simulations $S(x_i;\bar{\beta})$ were calculated using the posterior expectancy of parameter ($\bar{\beta}$).

3. Results and discussion

3.1. Environmental conditions

Detailed information on the seasonality of key environmental variables is essential to assess seasonal variation in the actual ET and its partitioning. The seasonal change in air temperature (T_a; °C), air vapor pressure deficit (D; kPa), net solar radiation (R_n; MJ m^{-2} d^{-1}), wind speed (u, m s^{-1}) at the height of 2 m, precipitation (mm), soil water content (θ; %) at the depth of 5 cm and leaf area index (LAI; m^2 m^{-2}) was illustrated in Fig. 2. During the study period (Days 157–273), the daily mean air temperature was around 9.5 °C, and the daily range of temperature was large, usually more than 15 °C (Fig. 2). The ecosystem experienced great day-to-day variation in daily mean D from 0.1 to 0.9 kPa. Also,

Table 1
Prior distributions and the parameter bounds for the S–W model. These values are derived from the literature; n/a indicates that information was not available in the literature. The posterior parameter distribution estimated by MCMC are based on observed data in our site, and are characterized by the mean and 95% CIs (i.e., 2.5th and 97.5th percentiles).

Parameter	Prior distribution			Posterior distribution				
	Lower Bound	Upper Bound	References	DOY157-173 (LAI < 3.0)	DOY174-243 (3.0 < LAI < 4.0)	DOY244-251 (2.0 < LAI < 3.0)	DOY252-273 (1.0 < LAI < 2.0)	Multi-data
g_{max} (mm s^{-1})	0	50	Kelliher et al. (1995)	36.6 (29.5, 49.0)	22.5 (20.4, 25.1)	12.3 (10.5, 15.0)	10.2 (10, 11.5)	18.2 (17.1,19.4)
Q_{50} (W m^{-2})	10	50	Leuning et al. (2008)	24.3 (11.3, 47.4)	16.8 (10.5, 31.0)	20.8 (10.7, 46.5)	17.9 (10.5, 42.1)	14.3 (10.3, 23.6)
D_{50} (kPa)	0.5	3	Leuning et al. (2008)	2.2 (1.3, 2.5)	2.4 (2.1, 2.5)	2.2 (1.5, 2.5)	0.8 (0.6, 1.1)	2.5 (2.3, 2. 8)
K_Q	0	1	Leuning et al. (2008)	0.51 (0.32, 0.80)	0.41 (0.31, 0.69)	0.50 (0.31, 0.78)	0.52 (0.31, 0.76)	0.46 (0.30, 0.58)
K_A	0	1	Leuning et al. (2008)	0.81 (0.56, 0.89)	0.85 (0.73, 0.90)	0.79 (0.57, 0.89)	0.86 (0.73, 0.90)	0.79 (0.84, 0.90)
b_1 (s m^{-1})	4.5	11.3	Sellers et al. (1992); Zhang (2012)	7.87 (6.15, 8.99)[a]				
b_2 (s m^{-1})	0	8	Sellers et al. (1992); Zhang (2012)	2.86 (0.41, 4.53)[a]				

[a] Calibrated using 2-week data in the middle of October during which the plant physiological activities were stopped.

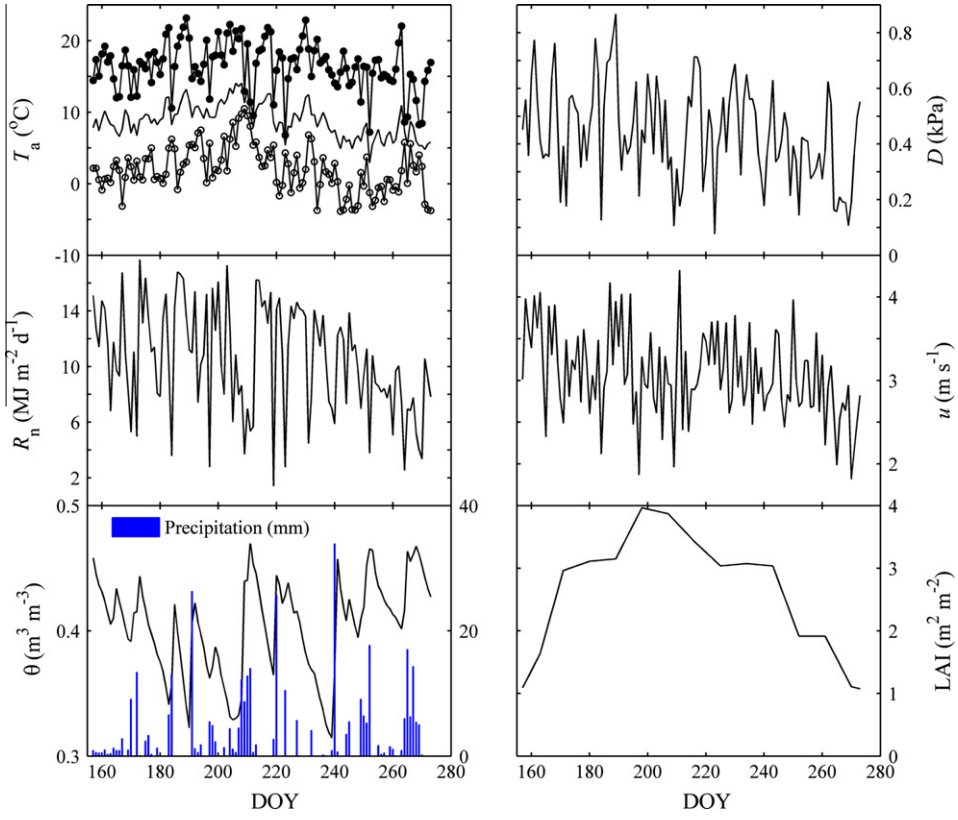

Fig. 2. Seasonal variation in daily air temperature (T_a) (mean air temperature, fine line; maximum air temperature, full circle; minimum air temperature, circle), mean daily air vapor pressure deficit (D), net solar radiation (R_n), wind speed (u) at the height of 2 m, precipitation (mm), soil water content (θ) at the depth of 5 cm and leaf are index (LAI).

half-hour data (not shown) indicated that peak values of D as high as 1.5–2 kPa frequently occurred in the afternoon (about 15:00 h at Beijing Standard Time). Daily mean wind speed ranged from 2 to 4 m s^{-1}, and was close to normal long-term values. The precipitation in year 2008 was 449 mm, which was comparable with the average value of 450 mm (Niu et al., 2008), and was mainly concentrated in the period from May to September. Within this high-precipitation period, 2–7 consecutive dry days occasionally followed rainy days (Fig. 2). During these short dry intervals, the soil water content decreased gradually from 0.45 m^3 m^{-3} to values close to 0.3 m^3 m^{-3} (Fig. 2).

The LAI increased rapidly from ~1 m^2 m^{-2} in early June to 3 m^2 m^{-2} on 22 June (DOY173), and reached a maximum of 4 m^2 m^{-2} on 17 July (DOY198). After the end of August (DOY243), the LAI decreased rapidly from about 3 m^2 m^{-2} to 1 m^2 m^{-2} (Fig. 2).

3.2. Posterior distribution of the S–W model parameters

As stated above, the parameters in the S–W model were associated with different components of ET (e.g., b_1 and b_2 were related to soil evaporation, and g_{max}, D_{50}, Q_{50} and K_Q were related to

transpiration). However, direct measurements of the components of ET (e.g., transpiration and evaporation) were not available at present study. Therefore, it may be unreasonable to simultaneously estimate all parameters in the S–W model. Here, two-day test period (in the late of October) was selected for which the plant physiological activities were stopped. Under such conditions the evaporation was regarded as mainly from the soil surface. By using the original Penman–Monteith equation which was adopted to express evaporation from soil surface (Zhang, 2012), we can get an independent estimate of the parameters (b_1 and b_2; s m^{-1}) in the soil surface resistance (r_{ss}; s m^{-1}). The posterior estimates for b_1 and b_2 corresponding to the means and 95% CIs (i.e., 2.5th and 97.5th percentiles) were 7.87 (6.15, 8.99) and 2.86 (0.41, 4.53), respectively (see details in Supporting information D). The soil surface resistance (r_{ss}; s m^{-1}) computed using the posterior mean parameter values and that (b_1 = 8.2, b_2 = 4.3) suggested by Sellers et al. (1992) were very similar (Supporting information D). In addition, evaporation (λE) calculated using the S–W model with the posterior mean parameter values were compared with measurements during the period 20–31 October. The linear regression between the measured and estimated λE values had a slope of 0.95, intercept of −6.36 W m^{-2} and a correlation coefficient of 0.76 (Supporting information D). Thus, we thought the estimates of the soil surface resistance parameters (b_1 and b_2; s m^{-1}) were proper and maintained constant during the whole study period.

By fixing the soil resistance parameters, other parameters (g_{max}, D_{50}, Q_{50}, K_A and K_Q) in the S–W model were calibrated with different seasonal dataset and multi-dataset procedures. Their posterior distributions corresponding to the means and 95% CIs were presented in Fig. 3. Such representation makes it possible to visualize seasonal differences of the posterior distributions of the parameters, while the shape of the plot reveals the dispersion and symmetry of the marginal distributions (Lehuger et al., 2009). It was noticed that the posterior distributions of most parameters (e.g., g_{max}, D_{50}, K_A and K_Q) become narrower compared to the uniform prior distributions (Fig. 3 and Table 1), which is undoubtedly due to the efficiency of our calibration procedure. Thus, the choice of an uniform prior distribution had little influence on the calibration, as the information contained in the experimental data gradually became dominant (Van Oijen et al., 2005). Noticeably, significantly seasonal variation in g_{max} was detected by the MCMC method based on different seasonal dataset (Fig. 3 and Table 1). That is, the maximum value occurred during initial leaf expansion period (DOY157-173) and declined after that (Fig. 3). Similar patterns have been found in a Populus forest (Zhu et al., 2011), a northern temperate grassland (Wever et al., 2002) and a Japanese grassland (Saigusa et al., 1998). In addition, the smallest value of D_{50} of DOY252-273 was mainly contributed to the relatively lower air vapor pressure deficit during this period (Fig. 2). On the contrary, parameter Q_{50} remained spread across their prior range of variation, and its posterior means were similar to the means specified by its prior distribution (about 25 W m^{-2}). This means that the calibration did not significantly reduce its uncertainty under the non-informative prior (Zhu et al., 2011).

The rightmost plot in each graph in Fig. 3 depicts the distribution obtained with the multi-data procedure. The shape of this plot and its median value appeared to be more constrained by certain datasets than others, which may be explained by the fact that the combination of such datasets had a comparatively larger number of observations, and subsequently gained more weight in the likelihood function (Lehuger et al., 2009). For example, the mean of g_{max} for the multi-dataset exhibited high similarity to that for DOY174-243 and DOY244-251, and D_{50} for the multi-dataset seemed to be more contained by DOY174-243 (Fig. 3).

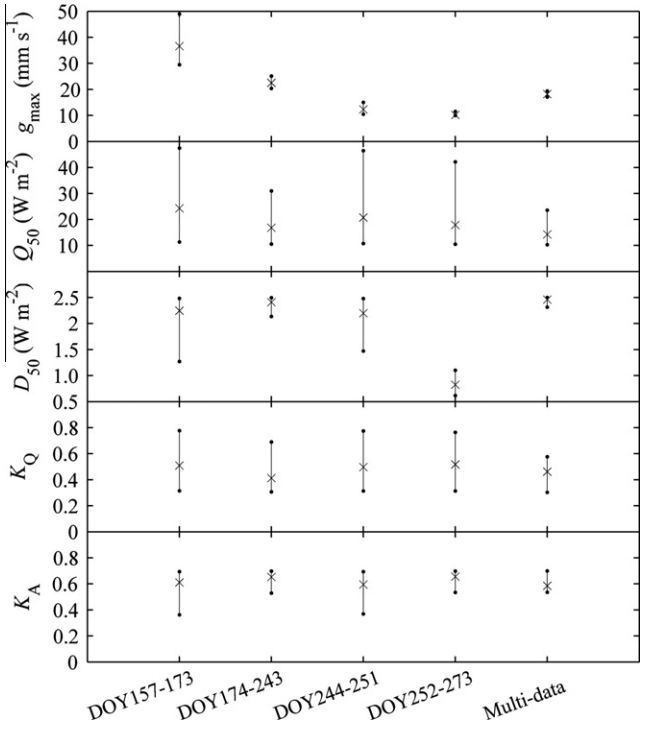

Fig. 3. Posterior mean estimates (cross) and 95% CIs (closed circles) for seasonal variation given by the Bayesian approach based on different dataset.

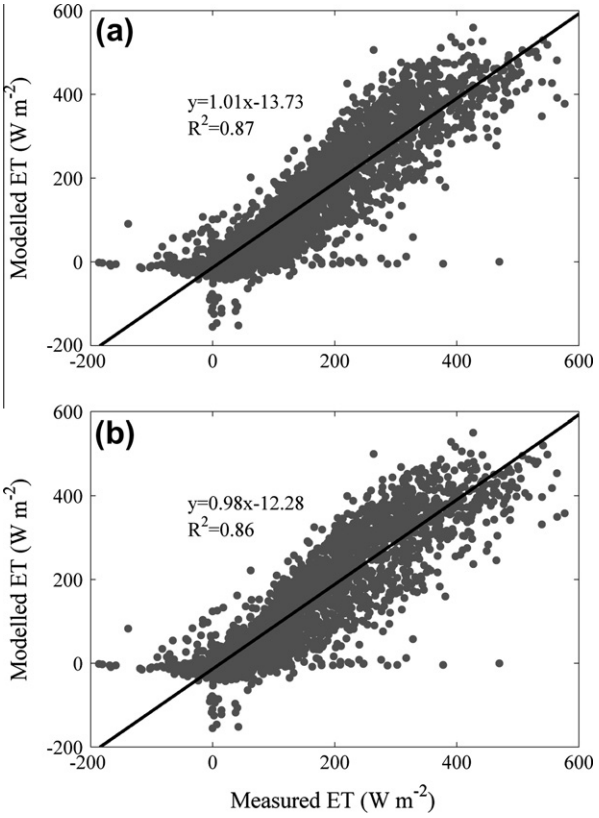

Fig. 4. Regression between measured and modeled half-hourly evapotranspiration values by different dataset procedures: (a) dataset-by-dataset procedure and (b) multi-dataset procedure. The regressions are: $y = 1.01x - 13.73$ ($R^2 = 0.87$) and $y = 0.98x - 12.28$ ($R^2 = 0.86$) for dataset-by-dataset and multi-dataset procedures, respectively.

3.3. Overall performance of the Bayesian method for the S–W model

Having parameterized the S–W model as described above (including both the dataset-by-dataset and multi-dataset procedures), we ran the model to simulate the half-hourly ET values (λET). The resulting simulations of λET using optimized parameters based on different datasets were compared with measured values (Fig. 4). However, it was noticed that the S–W model produced a slightly better fit to the half-hourly λET for all seasons when dataset-by-dataset optimized parameters were considered. Points in the plots of observed-versus-predicted λET fell tightly along the 1:1 line (slope = 0.97, 1.02, 1.01 and 0.97 with R^2 = 0.82, 0.88, 0.89 and 0.85 for DOY157-173, DOY174-243, DOY244-251 and DOY252-273, respectively; Table 2). Also, no obvious deviation of the diurnal simulations was detected in these four phases (Fig. 5a).

On the contrary, the error when using multi-dataset optimized parameters was not negligible during the leaf expansion (DOY157-173) and senescence periods (DOY252-273) (slope = 0.87 and 1.17 with R^2 = 0.80 and 0.85 for DOY157-173 and DOY252-273, respectively; Table 2). In general, the values of ET was slightly underestimated and overestimated by the multi-dataset procedure during the leaf expansion period and senescence period (Table 2 and Fig. 5b), respectively. This seems to be due to the significant differences in estimates of g_{max} between the dataset-by-dataset and multi-dataset procedures during these two phases (Fig. 3). Previous studies also have shown that systematic overestimation or underestimation of ET may occur when constant parameters were used for some ecosystems (Hu et al., 2009; Zhu et al., 2011). Thus, for long time simulations of ET, it was important to consider the seasonal changes in the physiology-related parameters (e.g., the maximum stomatal conductance, g_{max}).

3.4. Partitioning of ET and its controlling factors

The average daily evaporation and transpiration fluxes were illustrated in Fig. 6a. Transpiration was much greater than evaporation except during the leaf expansion (DOY157-173) and senescence periods (DOY252-273), when plants were less active. The

Table 2
Root mean square error (RMSE) of half-hourly evapotranspiration estimate, as well as the slope, intercept and coefficient of determination (R^2) of regression between measured and modeled half-hourly evapotranspiration values based on the posterior expectancy of parameters from the dataset-by-dataset and multi-dataset of the MCMC procedure for the S–W model.

Period	Dataset-by-dataset				Multi-dataset			
	Slope	Intercept	R^2	RMSE	Slope	Intercept	R^2	RMSE
DOY157-173 (LAI < 3)	0.97	−10.83	0.82	51.80	0.87	−9.75	0.80	53.40
DOY174-243 (LAI > 3)	1.02	−16.14	0.88	49.78	0.99	−15.83	0.88	49.94
DOY244-251 (2 < LAI < 3)	1.01	−11.97	0.89	37.76	1.08	−12.09	0.89	39.37
DOY252-273 (LAI < 2)	0.97	−8.56	0.85	32.69	1.17	−8.62	0.85	39.04
Whole season	1.01	−13.73	0.87	46.60	0.98	−12.28	0.86	47.95

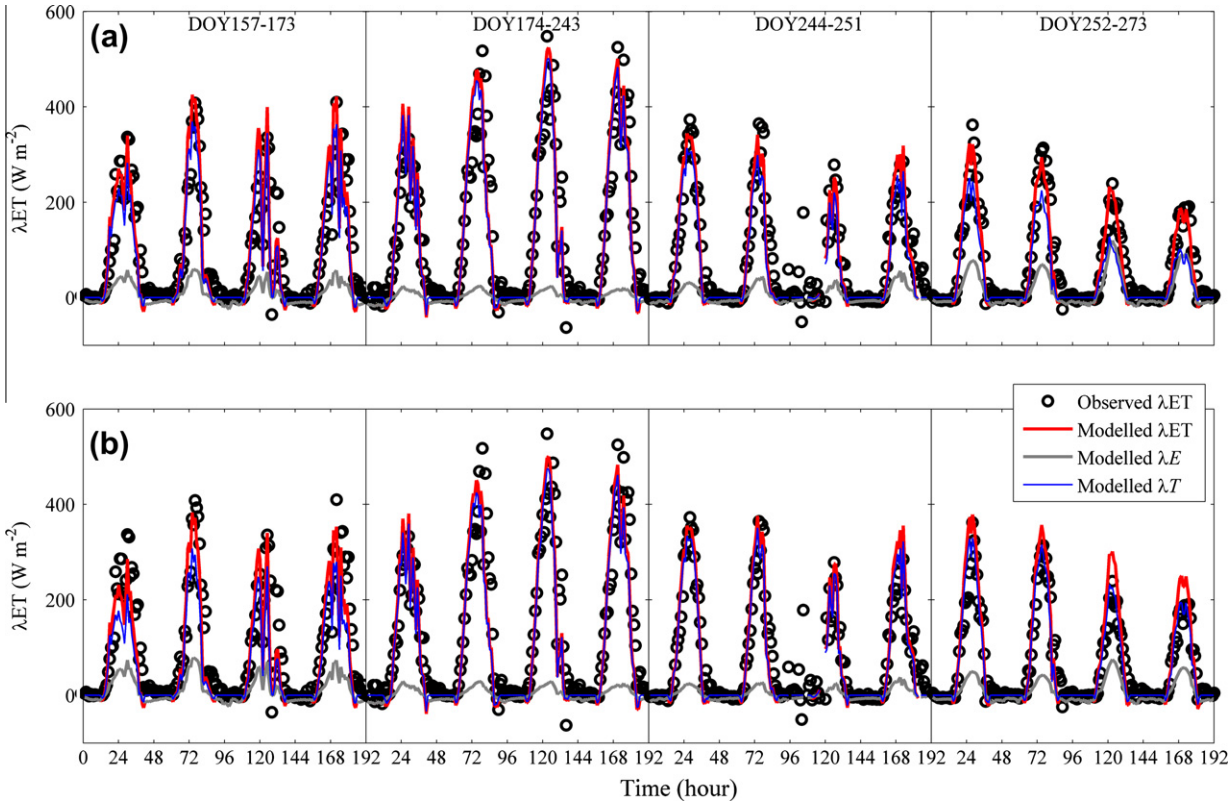

Fig. 5. Diurnal variations of the measured (circle) and modeled evapotranspiration (ET) during four distinct growing stages using different parameterized procedures: (a) dataset-by-dataset procedure and (b) multi-dataset procedure.

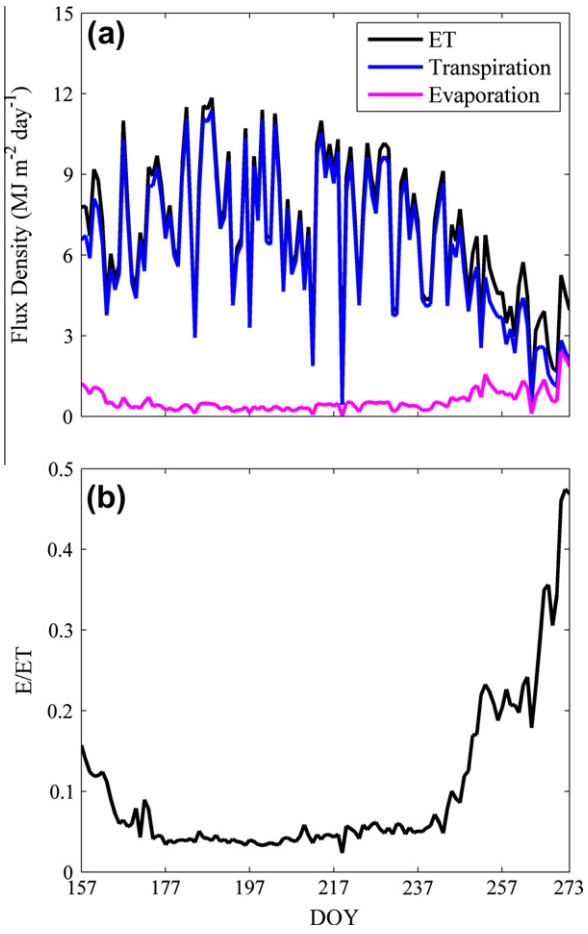

Fig. 6. (a) Daily variations in modeled evapotranspiration compared to transpiration and evaporation, and (b) ratio of evaporation to evapotranspiration estimated from the S–W model at the alpine grassland during the study period.

ratio of the estimated daily soil evaporation (E) over total evapotranspiration (ET) (E/ET) of peak growing seasons (DOY174-243) was 0.02–0.07 with a mean of 0.04 when LAI was higher than 3 m^2 m^{-2} (Fig. 6b). Thus, we conclude that water for soil surface evaporation in the alpine grassland ecosystem was small or negligible when the canopy was full developed. This trend of fractions of E in ET is in agreement with previous studies. For example, Wang and Yakir (2000) found E/ET is 0.015–0.035 over a mature wheat in arid and semi-arid environment. Ferretti et al. (2003) estimated E/ET over a short-grass steppe through measurements by stable isotopes in semi-arid northeastern Colorado. They found the daily E/ET ranged from nil to 0.13 with a mean of 0.07 during the growing season. Sauer et al. (2007) also found that the daily E/ET was less than 0.08 over a soybean crop when the canopy become close (LAI > 5 m^2 m^{-2}). Xu et al. (2008) investigated the daily dynamics of E/ET in a subalpine shrub-land (*Quercus aquifolioides*) based on stable isotopic measurements during three days in the early monsoon period in Wolong Nature Reserve, China. Their results indicated that daily E/ET was only about 0.02–0.05.

To understand the mechanisms in controlling E/ET, we investigated the effect of canopy conductance (g_{sc}) on the diurnal variations in E/ET with half-hourly data during the whole study period (Fig. 7a). As expected, the canopy conductance had significant effects on the diurnal variation in E/ET at the alpine grassland ecosystem. E/ET descended gradually with the increase of g_{sc} due to the combined effects of VPD, R_n, soil water content and plant physiological rhythm (Hu et al., 2009). It was noticed that a minor increase of g_{sc} would cause substantial decrease in E/ET when g_{sc} was at low level (less than 30 mm s^{-1}). But when g_{sc} exceeded this threshold, E/ET almost kept constant (5%) without further decrease (Fig. 7a). Similar phenomena were also discovered in other grassland ecosystems in China (Hu et al., 2009). The daily dynamic of E/ET was mainly controlled by the changes in LAI, and the relationship between E/ET and LAI in the alpine grassland can be described with a logarithmic function (Fig. 7b). That is, E/ET reduced gradually with the increase of LAI when LAI was less than 3 m^2 m^{-2}, and finally approached a constant value (about 0.05). This was consistent with previous studies (e.g., Liu et al., 2002; Kato et al., 2004; Hu et al., 2009). Compared with other grasslands in China (Hu et al., 2009), the sensitivity (i.e., the slope of the fixed curve) of E/ET to LAI was relative low (about −0.14). This may be due to the high vegetation cover (more than 95%) and good growth conditions of the alpine grassland. Interestingly, the sensitivity of E/ET to LAI was found to be considerably different between DOY157-198 (LAI increasing from 1.1 to 4.0) and DOY199-304 (LAI decreasing form 4.0 to 1.0). The slopes of the fit line between LAI and E/ET were −0.04 and −0.12 for DOY157-198 and DOY199-304, respectively, suggesting an increased sensitivity with the decline of vegetation conditions (i.e., leaf chlorophyll content).

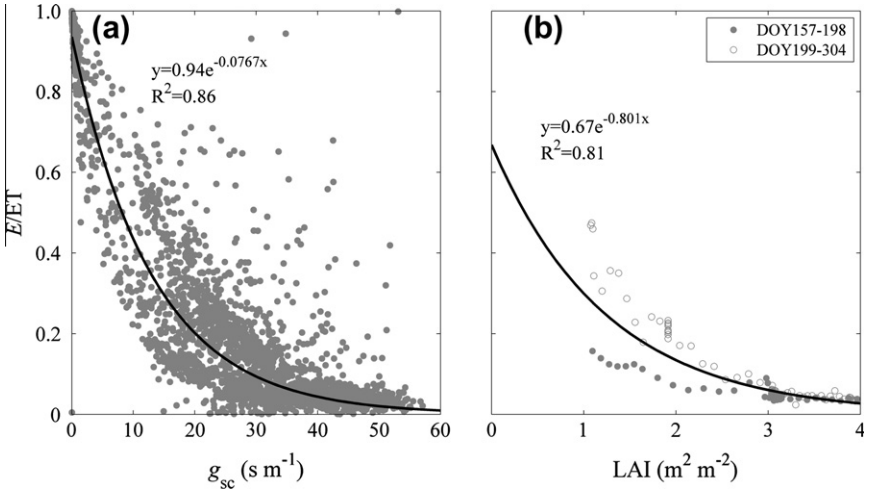

Fig. 7. (a) Effect of canopy stomatal conductance (g_{sc}) on E/ET at the half-hour time scale, and (b) effect of leaf area index (LAI) on daily E/ET. E/ET was calculated as the ratio of modeled daily E to modeled daily ET.

4. Conclusions

The study presented here illustrated the use of the Bayesian approach for the statistical analysis of a two-source ET model in the alpine grassland on Qinghai-Tibetan plateau. The good liner regression between simulations by the ET model using the posterior mean parameters obtained by different procedures (dataset-by-dataset and multi-data) and observations indicated that the model was very reliable in estimating the ET at the ecosystem level. However, some mismatches may exist for the multi-data procedure, due to the ignoring of seasonal variations of physiology-related parameters. Furthermore, canopy conductance, LAI as well as vegetation condition were the main factors control the partitioning of ET at different timescales. However, due to the lack of direct measurements on the different components of ET, the simultaneous estimates of all parameters were not achieved at present studies. Thus, combining methods (e.g., stable isotopes and EC) should be used in the future studies to get direct measurements of the different components of ET.

Acknowledgements

This research was supported by National Natural Science Foundation of China (Nos. 41001242, 40925004 and 40701054), New Century Excellent Talents in University of Chinese Ministry of Education (No. NCET-11-0219), Fundament Research for the Central University, Key Grant Project of Chinese Ministry of Education (Nos. 310005, 860857), and Foundation of Center for Dryland Water Resources Research and Watershed Science, Lanzhou University.

Appendix A. Supplementary material

Supplementary data associated with this article can be found, in the online version, at http://dx.doi.org/10.1016/j.jhydrol.2012.10.006.

References

Allen, R.G., Pereira, L.S., Raes, D., Smith, M., 1998. Crop Evapotranspiration – Guidelines for Computing Crop Water Requirements. FAO Irrigation and Drainage Paper, No. 56, FAO, Rome.

Chang, Z.Q., Feng, Q., Si, J.H., Su, Y.H., Xi, H.Y., Li, J.L., 2009. Analysis of the spatial and temporal changes in soil CO_2 flux in alpine meadow of Qilian Mountain. Environ. Geol. 58, 483–490.

Clark, J.S., Gelfand, A.E., 2006. A future for models and data in environmental science. Trends Ecol. Evol. 12, 375–380.

Ferretti, D.F., Pendall, E., Morgan, J.A., Nelson, J.A., LeCain, D., Mosier, A.R., 2003. Partitioning evapotranspiration fluxes from a Colorado grassland using stable isotopes: seasonal variations and ecosystem implications of elevated atmospheric CO_2. Plant Soil 254, 291–303.

Fisher, J.B., Whittaker, R.J., Malhi, Y., 2011. ET come home: potential evapotranspiration in geographical ecology. Glob. Ecol. Biogeogr. 20, 1–18.

Gasca-Tucker, D.L., Acreman, M.C., Agnew, C.T., Thompson, J.R., 2007. Estimating evaporation from a wet grassland. Hydrol. Earth Syst. Sci. 11 (1), 270–282.

Gelfand, A.E., Smith, A.F.M., 1990. Sampling-based approaches to calculating marginal densities. J. Am. Stat. Assoc. 85, 398–409.

Gelman, A., Rubin, D.B., 1992. Inference from iterative simulation using multiplesequences. Stat. Sci. 7, 457–511.

Gelman, A., John, C., Hal, S., Donal, R., 1995. Bayesian Data Analysis. Chapman & Hall.

Hastings, W.K., 1970. Monte Carlo sampling methods using Markov chains and their applications. Biometrika 57, 97–109.

Hu, Z.M., Yu, G.R., Zhou, Y.L., Sun, X.M., Li, Y.N., Shi, P.L., Wang, Y.F., Song, X., Zheng, Z.M., Zhang, L., Li, S.G., 2009. Partitioning of evapotranspiration and its controls in fourgrassland ecosystems: Application of a two-source model. Agric. Forest Meteorol. 149, 1410–1420.

Iritz, Z., Lindroth, A., Heikinheimo, M., Grelle, A., Kellner, E., 1999. Test of a modified Shuttleworth–Wallace estimate of boreal forest evaporation. Agric. Forest Meteorol. 98–99, 605–619.

Jarvis, P.G., 1976. The interpretation of the variations in leaf water potential and stomatal conductance found in canopies in the field. Philosophical Transactions of the Royal Society of London. Series B 273, 563–610.

Jung, M., Reichstein, M., Ciais, P., Seneviratne, S.I., Sheffield, J., Goulden, M.L., Bonan, G., Cescatti, A., Chen, J.Q., de Jeu, R., Dolman, A.J., Eugster, W., Gerten, D., Gianelle, D., Gobron, N., Heinke, J., Kimball, J., Law, B.E., Montagnani, L., Mu, Q.Z., Mueller, B., Oleson, K., Papale, D., Richardson, A.D., Roupsard, O., Running, S., Tomelleri, E., Viovy, N., Weber, U., Williams, C., Wood, E., Zaehle, S., Zhang, K., 2010. Recent decline in the global land evapotranspiration trend due to limited moisture supply. Nature 467, 951–954.

Kato, T., Kimura, R., Kamichika, M., 2004. Estimation of evapotranspiration, transpiration ratio and water-use efficiency from a sparse canopy using a compartment model. Agric. Water Manag. 65 (3), 173–191.

Kelliher, F.M., Leunig, R., Raupach, M.R., Schulze, E.D., 1995. Maximum conductances for evaporation from global vegetation types. Agric. Forest Meteorol. 73, 1–16.

Larssen, T., Huseby, R.B., Cosby, B.J., Host, G., Hogasen, T., Aldrin, M., 2006. Forecasting acidification effects using a Bayesian calibration and uncertainty propagation approach. Environ. Sci. Technol. 40 (24), 7841–7847.

Lehuger, S., Gabriellea, B., van Oijenb, M., Makowskic, D., Germond, J.C., Morvane, T., Hénaultd, C., 2009. Bayesian calibration of the nitrous oxide emission module of an agro-ecosystem model. Agric. Ecosyst. Environ. 133, 208–222.

Leuning, R., Zhang, Y.Q., Rajaud, A., Cleugh, H., Tu, K., 2008. A simple surface conductance model to estimate regional evaporation using MODIS leaf area index and the Penman–Monteith equation. Water Resour. Res. 44, W10419. http://dx.doi.org/10.1029/2007WR006562.

Li, X., Li, X.W., Li, Z.Y., Ma, M.G., Wang, J., Xiao, Q., Liu, Q.H., Che, T., Chen, E.X., Yan, G.J., Hu, Z.Y., Zhang, L.X., Chu, R.Z., Su, P.X., Liu, Q.H., Liu, S.M., Wang, J.D., Niu, Z., Chen, Y., Jin, R., Wang, W.Z., Xin, Z.Z., Ren, H.Z., 2009. Watershed allied telemetry experimental research. J. Geophys. Res. 114, D22103. http://dx.doi.org/10.1029/2008JD011590.

LI-COR Inc., 2000. LI-7500 CO_2/H_2O Analyzer Instruction Manual. LI-COR Inc., Lincoln, NE.

Liu, X., Chen, B., 2000. Climatic warming in the Tibetan Plateau during recent decades. Int. J. Climatol. 20, 1729–1742.

Liu, C.M., Zhang, X.Y., Zhang, Y.Q., 2002. Determination of daily evaporation and evapotranspiration of winter wheat and maize by large-scale weighing lysimeter and micro-lysimeter. Agric. For. Meteorol. 111 (2), 109–120.

Mauder, M., Foken, T., 2004. Documentation and instruction manual of the eddy covariance software package TK2. Universität Bayreuth, Abt. Mikrometeorologie, Arbeitsergebnisse (Print, ISSN 1614-8916; Internet, ISSN 1614-8926).

Metropolis, N.R., Rosenbluth, A.W., Rosenbluth, M.N., Teller, A.H., 1953. Equations of state calculations by fast computing machines. J. Chem. Phys. 21, 1087–1091.

Monteith, J.L., 1965. Evaporation and environment. Symp. Soc. Exp. Biol. 19, 205–234.

Moran, M.S., Scott, R.L., Keefer, T.O., Emmerich, W.E., Hernandez, M., Nearing, G.S., Paige, G.B., Cosh, M.H., O'Neill, P.E., 2009. Partitioning evapotranspiration in semiarid grassland and shrubland ecosystems using time series of soil surface temperature. Agric. For. Meteorol. 149 (1), 59–72.

Niu, Y., Liu, X.D., Luo, Y.Z., Yan, J.L., Luo, L.F., 2008. Microclimate characteristics of alpine grassland in Qilian Mountains. Grassland Turf 126 (1), 59–69 (in Chinese with English Abstract).

Reinds, G.J., van Oijen, M., Heuvelink, G.B.M., Kros, H., 2008. Bayesian calibration of the VSD soil acidification model using European forest. Geoderma 146, 475–488.

Reynolds, J.F., Kemp, P.R., Tenhunen, J.D., 2000. Effects of long-term rainfall variability on evapotranspiration and soil water distribution in the Chihuahuan desert: a modeling analysis. Plant Ecol. 150, 145–159.

Saigusa, N., Takehisa, O., Liu, S., 1998. Seasonal variations of the exchange of CO_2 and H_2O between a grassland and the atmosphere: an experimental study. Agric. For. Meteorol. 89, 131–139.

Samanta, S., Mackay, D.S., Clayton, M.K., Kruger, E.L., Ewers, B.E., 2007. Bayesian analysis for uncertainty estimation of a canopy transpiration model. Water Resour. Res. 43, W04424. http://dx.doi.org/10.1029/2006WR005028.

Sauer, T.J., Singer, J.M., Prueger, J.H., DeSutter, T.M., Hatfield, J.L., 2007. Radaition balance and evaporation portioning in a narrow-woe soybean canopy. Agric. Forest Meteorol. 145, 206–214.

Sellers, P.J., Heiser, M.D., Hall, F.G., 1992. Relations between surface conductance and spectral vegetation indices at intermediate ($100\ m^2$ to $15\ km^2$) length scales. J. Geophys. Res. 97 (D17), 19033–19059.

Shugart, H.H., 2000. Ecosystem modeling. In: Sala, O.E., Jackson, R.B., Mooney, H.A., Howarth, R.W. (Eds.), Methods in Ecosystem Science. Springer, New York, pp. 373–388.

Shuttleworth, W.J., Gurney, R.J., 1990. The theoretical relationship between foliage temperature and canopy resistance in sparse crops. Quart. J. Roy. Meteorol. Soc. 116, 497–519.

Shuttleworth, W.J., Wallace, J.S., 1985. Evaporation from sparse crops – an energy combination theory. Quart. J. Roy. Meteorol. Soc. 111, 839–855.

Svensson, M., Jansson, P.E., Gustafson, D., Kleja, D.B., Langvall, O., Lindroth, A., 2008. Bayesian calibration of a model describing carbon, water and heat fluxes for a Swedish boreal forest stand. Ecol. Model. 213, 331–344.

Thompson, N., Barrie, M., Ayeles, A., 1981. The meteorological office rainfall and evapotranspiration calculation system: MORECS. Hydrological Memorendum 45, 69 p.

Van Oijen, M., Rougier, J., Smith, R., 2005. Bayesian calibration of process-based forest models: bridging the gap between models and data. Tree Physiol. 25 (7), 915–927.

Vorosmarty, C.J., Federer, C.A., Schloss, A.L., 1998. Potential evaporation functions compared on US watersheds: possible implications for global-scale water balance and terrestrial ecosystem modeling. J. Hydrol. 207, 147–169.

Wang, X.F., Yakir, D., 2000. Using stable isotopes of water in evapotranspiration studies. Hydrol. Process. 14, 1407–1421.
Wever, L.A., Flanagan, L.B., Carlson, P.J., 2002. Seasonal and interannual variation in evapotranspiration, energy balance and surface conductance in a northern temperate grassland. Agric. For. Meteorol. 112 (1), 31–49.
Williams, D.G., Cable, W., Hultine, K., Hoedjes, J.C.B., Yepez, E.A., Simonneaux, V., Er-Raki, S., Boulet, G., de Bruin, H.A.R., Chehbouni, A., Hartogensis, O.K., Timouk, F., 2004. Evapotranspiration components determined by stable isotope, sap flow and eddy covariance techniques. Agric. Forest Meteorol. 125 (3–4), 241–258.
Xu, C.Y., Singh, V.P., 1998. A review on monthly water balance models for water resources investigations. Water Resour. Manage. 12, 31–50.
Xu, Z., Yang, H.B., Liu, F.D., An, S.Q., Cui, J., Wang, Z.S., Liu, S.R., 2008. Partitioning evapotranspiration flux components in a subalpine shrubland based on stable isotopic measurements. Bot. Stud. 49, 351–361.
Zhang, X., 2012. Improvement of a soil-atmosphere-transfer model for the simulation of bare soil surface energy balances in semiarid areas. Asia-Pacific J. Atmos. Sci. 48 (1), 97–105.
Zhou, M.C., Ishidaira, H., Hapuarachchi, H.P., Magome, J., Kiem, A.S., Takeuchi, K., 2006. Estimating potential evapotranspiration using Shuttleworth–Wallace model and NOAA-AVHRR NDVI data to feed a distributed hydrological model over the Mekong River basin. J. Hydrol. 327, 151–173.
Zhu, G.F., Li, X., Su, Y.H., Lu, L., Huang, C.L., 2011. Seasonal fluctuations and temperature dependence in photosynthetic parameters and stomatal conductance at the leaf scale of *Populus euphratica Oliv*. Tree Physiol. 31 (2), 178–195.